Influence of Graphene Oxide on Asphaltene Nanoaggregates

Colloids and Surfaces A: Physicochemical and Engineering Aspects 630 (2021) 127614

Contents lists available at ScienceDirect

Colloids and Surfaces A: Physicochemical and Engineering Aspects

journal homepage: www.elsevier.com/locate/colsurfa

Influence of graphene oxide on asphaltene nanoaggregates

Govindan Induchoodan [a,b,*], Helen Jansson [b], Jan Swenson [a]

[a] Department of Physics, Chalmers University of Technology, SE-412 96 Göteborg, Sweden
[b] Department of Architecture and Civil engineering, Chalmers University of Technology, SE-412 96 Göteborg, Sweden

HIGHLIGHTS

- First study ever on the microstructure of graphene oxide-modified asphaltenes.
- Influence of graphene oxide on the structure of colloidal systems like bitumen.
- Detailed experimental study of interactions between graphene oxide and asphaltenes.
- Understanding of the consequence of using graphene oxide as demulsification agent.
- A detailed evaluation of the usability of graphene oxide as a bitumen modifier.

GRAPHICAL ABSTRACT

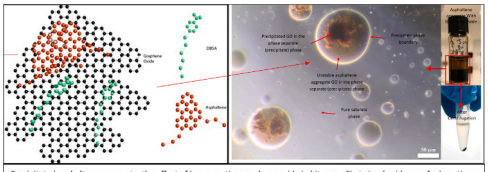

Precipitated asphaltene aggregate, the effect of incorporating graphene oxide in bitumen. First visual evidence of adsorption of asphaltene nanostructures on graphene oxide.

ARTICLE INFO

Keywords:
XPS
XRD
Asphaltene adsorption
Graphene oxide
Bitumen
Material enhancement

ABSTRACT

Asphaltenes are a group of exotic hydrocarbons found in bitumen and other forms of heavy crude oil derivatives. These hydrocarbons, with elusive chemistry, give crude oil derivatives (CODs), such as bitumen, its characteristic properties. In bitumen, they form stable aggregates by interacting with other molecules, called asphaltene aggregates. Attempts have been made to enhance bitumen with nanoparticles, like graphene derivatives. Such studies have been successful in displaying the enhanceability of bitumen, but no studies have been directly focused on how the structural stability of asphaltene aggregates present in bitumen is affected by the incorporation of nanoparticles. The phase stability of the asphaltene aggregates is a pertinent question, which is often ignored. In this study, we investigate the physical impact of incorporating graphitic nanoparticles on the structure of bitumen. For this, we utilise graphene oxide (GO). GO is a form of polyaromatic nanoparticle with a similar structure to asphaltenes, such that both have molecular defects induced by heteroatoms. We have experimentally investigated the structural stability of the asphaltenes, using XPS, XRD and SEM-EDX to elucidate the interaction between asphaltenes and GO, and its implications for the stability of bitumen used for e.g., the surface layer of roads. In roads, asphaltene aggregates exist as stable structures, until GO has been introduced. The experimental results show that the introduction of GO initiates destabilisation of the asphaltene aggregates, and we discuss the destabilisation mechanism in this paper. Thereby, we conclude that counter intuitively, the introduction of graphene or GO has a negative impact on the structure of bitumen, thus hindering any functional enhancements to bituminous roads.

Abbreviations: GO, graphene oxide; DBSA, dodecylbenzene sulfonic acid; SEM, scanning electron microscope; EDX, Energy-dispersive X-ray spectroscopy; XPS, x-ray photoelectron spectroscopy; TLC-FID, thin layer chromatography- flame ionisation detection; XRD, x-ray diffraction; FTIR, fourier-transform infrared spectroscopy; CNAC, critical nanoaggregate concentration; CCC, critical clustering concentration.

* Corresponding author at: Department of Physics, Chalmers University of Technology, SE-412 96 Göteborg, Sweden.
E-mail address: govindan@chalmers.se (G. Induchoodan).

https://doi.org/10.1016/j.colsurfa.2021.127614
Received 11 June 2021; Received in revised form 25 August 2021; Accepted 20 September 2021
Available online 28 September 2021

1. Introduction

Bitumen is a well-known and comprehensively studied colloidal system, with a viscosity of nearly a million pascal-seconds (Pa·s) [1]. However, even with such a high viscosity, bitumen is a fluid. One important component in bitumen is the asphaltenes, which exists in the form of stable aggregates [2]. Asphaltenes are a class of complex poly-aromatic hydrocarbons and a naturally occurring graphitic structure with molecular defects, including heteroatomic and other basic sites [3]. Despite that asphaltenes have been widely studied, their precise structure is still a subject of debate [4–6]. Researchers have used characterisation techniques such as spectroscopy, diffraction, microscopy and chromatography to characterise the structure of asphaltenes [7–23]. The results indicate 3 possible chemical network structures, the so-called i) island ii), archipelago and iii) aryl-linked structures, where the dominant network structure is the island structure with minor fractions of the archipelago and aryl-linked structures [5].

In a recent publication, Chen et al. [5], presented atomic force microscope images of the island structure of asphaltenes. The results indicate that asphaltenes have a single polycyclic aromatic structure with an average size of 7 rings, where about 50% of the asphaltene structure is aromatic while the remaining of the structures are alicyclic and open-chain aliphatic, with alkanes existing in the form of end-functionalised structures [5]. In addition, mass spectroscopy studies have shown that asphaltenes have a high concentration of heteroatoms, probably the highest of any petroleum fractions [10–14]. The heteroatoms, consisting of carbon (C), hydrogen (H), oxygen (O), nitrogen (N) and sulphur (S), are predicted to exist as CHO, CHOS, CHNO and CHNOS molecular series, with an average H/C ratio of 1.75 and a C/O ratio of 0.15 [10–14].

Critical nanoaggregate concentration (CNAC) and critical clustering concentration (CCC) have been used as thresholds to predict the aggregation behaviour of asphaltenes [5,22–29]. It is highly likely that these asphaltenes form layered structures through mutual interaction to form nanoaggregates [5]. These nanoaggregates have a size of approximately 2 nm and are formed when an asphaltene aggregation number of about 7 molecules is reached. It is also displayed through experimental examination that the nanoaggregates form clusters on a longer length scale of about 5 nm when they reach an aggregation number of nearly 10 nanoaggregates. When the cluster size exceeds the CCC, there will be a phase separation.

In crude oil, the asphaltene nanoaggregates interact with less polar molecules called resins, that act as surfactants, to form larger aggregates structures, i.e., asphaltene aggregates. The stability of the asphaltene aggregates is, except for the interaction with resins, also associated with the solubility parameter, evolution of violates, the ratio of other molecules to asphaltenes (other crude oil fractions) [27–29]. Thus, by inhibiting the asphaltene growth, more "stable aggregates'' can be produced [5,30,31]. The stability of asphaltene aggregates is crucial for the structure, and thereby also for the properties of the bulk material, i.e., bitumen. Bitumen is the name provided to identify a specific ratio of saturates, aromatics, resins and asphaltenes, the so-called SARA fractions [2]. With its high viscosity, bitumen is the most viscous crude oil derivative (COD), categorising it as a heavy COD [1]. It is the asphaltene aggregates that mainly contribute to the viscosity of heavy CODs.

The production and transportation of heavy CODs, such as bitumen, has become increasingly important [32–44]. Since, bitumen is strongly adhesive and resistant to water it is commonly used as the surface layer of roads. To be able to transport bitumen, and for workers to be able to lay roads, bitumen has to be less viscous. This means that bitumen has to be maintained at high temperatures (150–180 °C) and, consequently, produced close to the working site. This processing/transporting technique is therefore both energy demanding and inefficient.

In general, two methods are used as an alternative to the conventional transportation method. Those are deasphalting and emulsification [32]. By deasphalting heavy CODs, larger structures, such as asphaltenes are removed to reduce the viscosity [32–37]. However, heavy CODs such as bitumen obtains its wanted properties, e.g., viscosity and viscoelasticity, from the asphaltene aggregates [32], and by the removal of the asphaltenes, its most important properties are lost. In emulsification, the heavy CODs are dispersed in water as droplets stabilized by surfactants [33], which results in a reduction of the viscosity. In this case, the asphaltene aggregates contribute to forming stable water-in-oil emulsions [32–37]. The formation of a viscoelastic, physically cross-linked asphaltene aggregate network at the water/oil interface determines the stability of these emulsions [36].

Polymers, surfactants, ionic liquids and nanoparticles have been used to stabilise such emulsions [32–47] by tailor the stability, size and surface characteristics of the water-in-oil emulsions [44–47]. The typical properties of nanoparticles, such as high surface area, high thermal and mechanical stability, good mobility in porous media and turnability for task-specific needs have made them attractive components in emulsions for applications [38–47]. The most commonly used nanoparticles ranges from inorganics, organic-inorganic and organic nanoparticles and include, for example, silica-based particles, NiO/poly (DVB) HIPE, iron-oxide/Chitosan, NiO/ZSM-5a, NiO/AlPO-5, Cardanol/SiO2, carbon nanotubes (CNTs), iron oxide-CNTs and graphene oxide (GO) [32,33,36, 38–47]. In, for instance, the crude oil industry, organic nanoparticles, such as CNTs and graphene, have been used to induce an adsorption of asphaltenes [36].

From a molecular dynamic (MD) simulation it was demonstrated that $\pi - \pi$ interactions, i.e., attractive, noncovalent interactions between aromatic rings, between asphaltenes and carbon nanotubes are the main reason for asphaltene adsorption on the nanoparticles [36]. The same kind of interaction also occurs for graphene, due to graphene's delocalised π orbitals [48].

As described above, in saturates, asphaltenes form asphaltene aggregates by interacting with amphiphiles such as resins [2–4,49–65]. The amphiphiles stabilize the asphaltene nanoaggregates by inhibiting the growth of asphaltene clusters and producing asphaltene aggregates with adsorbed amphiphiles on the surface through an acid-base interaction [49–65]. The asphaltene cores self-assemble through $\pi - \pi$ stacking, forming the nanoaggregates. These asphaltene nanoaggregates interact with less polar aromatic fractions in crude CODs, through hydrogen bonding and polar-polar interactions, to form stable structures. Resins (amphiphiles) along with aromatics (organic solvents) function together to help stabilize asphaltenes [49–65]. Asphaltenes stabilized by both these mechanisms are dispersed in the saturate phase of bitumen. It is this that leads to the complex nature of bitumen [1].

Recent studies have indirectly displayed the ability of GO to interact with asphaltenes in water-in-oil emulsions [38–43]. GO and asphaltenes have a similar structure, a graphitic structure with molecular defects. However, while asphaltenes are naturally occurring, GO is produced by introducing defects to a pristine graphitic structure, such as graphene. GO is a metastable derivative of graphene with induced defects in which the sp2 hybridised state is transformed to a sp3 hybridised state [48]. In GO, oxygen and carbon bond to form i) epoxy bridges and ii) hydroxyl groups in the bulk, and iii) pairwise carboxyl groups on the edges, and iv) islands of monoatomic thick graphitic domains [48]. This transformation makes GO both reactive and polar. This means that apart from the $\pi - \pi$ interaction of graphene, GO can also form hydrogen bonds and dipole moments with other molecules.

The effect of the introduction of graphitic particles on crude oil emulsions have been experimentally displayed [38–43]. In addition, calculations and simulations [41–43] have been performed to theorize the possible mechanism for demulsification of crude oil emulations. The general conclusions drawn from the results obtained by these studies, is that asphaltenes at the oil-water interface adsorb onto GO surfaces through an acid-base interaction, which causes an increase in the interfacial tension and eventual a phase separation of the emulsion.

Given the importance of asphaltene aggregates for the properties of bitumen, the adsorption of asphaltene aggregates onto GO and other

graphitic derivatives leads to three important questions.

a) The adsorption of asphaltene aggregates onto GO, does it have any impact on the structural reversibility of asphaltene aggregates?
b) What is the impact of adding GO as a demulsification agent to bitumen, and, in the long term, does it have any influence on the structure and properties of bitumen, post demulsification [32,33,36,38–47]?
c) If adding GO (or other graphene derivatives) lead to the removal of asphaltenes [38–47], through the adsorption onto GO, how does it then come that many researchers have reported an improvement in, for instance, thermal and mechanical properties of bitumen [66–77]?

To further elaborate, if nanoparticles, such as GO, can create a more favourable microstructure in bitumen, it could lead to superior applications. By this, large amounts of money, energy and resources can be saved since GO can first act as a demulsification agent and then proceed to form a favourable microstructure. Thus, it would allow engineers to extend properties like the durability, mechanical properties and thermal conductivity. On the other hand, if the normal asphaltene aggregate structure in bitumen is destroyed by phase separation and/or irreversible adsorption onto GO, then the entire function of bitumen will be lost as asphaltenes are the subfraction in bitumen that predominately influence the properties of bitumen.

A theorized model for the GO adsorption mechanism, based on the three points above, can have significant implications on the potential use of GO as a demulsification agent in bitumen-water emulsion and/or as a bitumen modifier. Thus, it is important to experimentally observe the theorised adsorption of asphaltenes on GO. It is equally significant to examine the reversibility and characteristics of the potential adsorption.

It should be noted that like asphaltenes, resins are chemically complex. Therefore, resins are often replaced by other simpler chemical molecules, of which 4-Dodecylbenzene sulfonic acid (DBSA), which is an acid of linear sodium dodecylbenzene sulfonate, is the most commonly used surfactant [49]. DBSA is an alkyl aryl sulfonate with a hydrophilic sulfonate acid and a 12-carbon tail [49]. It has previously been stated that the sulfonic acid head of DBSA will strongly interact with asphaltenes [49,51] and that, in non-polar solvents such as oils, electrostatic forces between the two species will dominate over other forms of interactions. Extracted asphaltenes can be redispersed with DBSA to produce an asphaltene aggregate system. DBSA reveals its effective amphiphiles for interaction with asphaltenes by an acid-base interaction. Numerous publications have shown that DBSA is more efficient in the interaction with asphaltenes compared to naturally found molecules in bitumen (such as resins)[49–65].

When DBSA molecules are dispersed in polar solvents, they will deprotonate. This leads to the formation of dodecyl benzenesulfonate. In such circumstances, polar−polar interactions, $\pi - \pi$ stacking, hydrogen bonds, and tail−tail interactions will become the main driving forces [62]. Bin Jiang et al. [62], postulate in their model that ionized DBSA can reduce asphaltene nanoaggregate clusters to monomeric cores, while Al-Sahhaf et al. [63], reported that a drastic increase in the amount of heptane is required to destabilize asphaltene aggregates produced by non-ionic DBSA. High-resolution transmission electron microscopy (HR-TEM) images of asphaltene aggregates by Goual et al. [49], show evidence of inverse prolate filament like aggregates at a concentration of 1000 ppm of DBSA. At a concentration of 10000 ppm of DBSA, these aggregates form long-range agglomerates [49]. In their work, Mahmoud Alhreez et al., [64] used a fraction of 4% DBSA and performed XRD and TEM analysis to display the size and characteristics of the asphaltene aggregates formed. Therefore, the same volume fraction of DBSA was also used in this study.

In this work we have experimentally investigated the theorized effect [38–43] of GO on asphaltene aggregates and the implications for the structural properties of bitumen. However, in order to experimentally study the effect of GO on the asphaltene aggregates (and then the implications for the properties of bitumen), it is necessary to isolate the influence of GO on the pure water-free asphaltene aggregate system. Therefore, the n-heptane insoluble asphaltene fraction (C7) was extracted from bitumen and used in the sample preparations [3,5,23,24,28]. It should be noted that the extracted asphaltene fraction is proposed to exist in a low energy state, i.e., in the form of nanoaggregates [2–6]. From the results it is obvious that asphaltenes adsorb on GO irreversibly and thereby GO will cause detrimental effects of bitumen properties, although the high viscosity of bitumen makes the physical interaction between GO and asphaltenes difficult to observe on a macroscopic scale.

2. Experimental section

2.1. Materials

For this study, M-grade XGnP graphene nanoplatelets (GnP), purchased from XGScience were used. The GnP has a surface area of 120–160 m^2g^{-1}, a thickness of 6–8 nm, a density of 2.2 $kgcm^{-3}$ and a diameter of 25 μm. Bitumen, obtained from Skanska Sweden AB, was used as a source for the asphaltene aggregate extraction. Analytical grade n-heptane (99.9%), n-hexane (99.9%), toluene (90%), hydrochloric acid (35%), potassium permanganate, sodium nitrate, sulfuric acid (95–97%) and hydrogen peroxide (35%) were purchased from Sigma Aldrich and Fisher Science.

2.2. Asphaltene nanoaggregate extraction

In order to increase the asphaltene content before the extraction, bitumen was aged in a so-called rolling thin-film oven test (RTFOT) setup [78] at 180 °C for 50 min. The aged bitumen was then heated and poured into an Erlenmeyer flask and weighed. Thereafter, n-heptane was added in a ratio of 100 ml to every 1 g of bitumen. A magnetic steerer was placed in the flask and the flask was subsequently placed in a sand bath. The entire set up was placed on a heating/magnetic steering plate and a Dimroth reflux condenser was placed on top of the Erlenmeyer flask, and then the entire setup was sealed using a lab clamp. After this, the reflux condenser was connected to a water supply with appropriate pressure. The bitumen solution was then heated to 95 °C and allowed to steer for 1 h, and the heater was thereafter turned off. The solution was poured into a 30 ml conical centrifuge tube and centrifuged at 4000 rpm for 5 min using a Sigma 4–16 centrifuge. The solution was decanted, and the precipitate was air dried for 24 h to ensure that the extracted material was completely dry of any solvent, including toluene and water molecules.

2.3. Preparation of GO

Graphite platelets (25 μm) were exfoliated using a shear-mixer. The shear-exfoliated graphite was converted into GO using the so-called “modified Hummers method”. Accordingly, 0.5 g graphene was mixed with 3 g potassium permanganate and 0.5 g sodium nitrate in the presence of 23 ml sulfuric acid and steered in an ice bath for 4 h. After which 46 ml of di-ionized water was introduced and the mixture was steered at 98 °C for 2 h. The mixture was thereafter allowed to cool, and 100 ml of sulfuric acid was then added. Thereafter also 50 ml of hydrogen peroxide was added. This mixture was thereafter filtered and 5% HCl was poured on the GO filter until the pH was neutral. A 20 μm filter was used post neutralisation to collect only larger flakes of GO from the dispersion.

2.4. Preparation of asphaltene aggregate system

0.5 g of 1 g/ml of DBSA was dispersed in 10 ml saturates to produce a micelle precursor with ~ 4.7% v/v (1:20 DBSA: saturates). 5 mg of asphaltene was dispersed in 1 ml of toluene. The dispersant was sonicated, centrifuged and dried under reduced pressure. Asphaltene was

thereafter dispersed in 5 ml of the DBSA micelle precursor. 5 mg of asphaltene was dispersed in 5 ml of the micelle precursor. The sample was vigorously shaken and sonicated for 15 min to produce the asphaltene aggregate system used for the experiments.

2.5. Preparation of GO incorporated asphaltene aggregate system

10 mg of GO was dispersed in 10 ml of methanol and sonicated for 45 min in a water bath, and thereafter centrifuged at 4500 rpm for 5 min. The process was repeated twice, and GO was then dried under reduced pressure to remove any residual water. A mixture of GO and asphaltene aggregates were prepared (with the same mass fraction as used in Section 2.4), by adding GO to 5 ml asphaltene aggregate system. The sample was vigorously shaken and sonicated for 15 min and then used for the experiments.

2.6. Transmission light microscopy

The transmission light microscopy was performed by an Olympus BX53 microscope. Prior to each measurement, a smaller amount of the asphaltene aggregate and the precipitate samples were placed on a glass slide. The microscope was operating in the transmission mode at an ambient temperature. Magnifications of 2X, 10X, 20X and 50X were used to observe the samples. In addition, brightfield, phase contrast, and polarised light modes were used for the measurements.

2.7. SEM-EDX imaging

A JEOL JSM 7800 FPrism (field emission gun) SEM was used for microscopy analysis. For these measurements, specimens were dispersed in hexane and washed 3 times to remove any residual saturates. The washed samples were dispersed on an activated silicon substrate and air dried before loading the sample into the microscope. The samples were analysed with an accelerating voltage of 2.5 kV. A lower electron detector was used to obtain the electrons generated in the secondary electron analysis.

EDX is a method to analyse surface elemental composition. The technique is based on the Kα radiation of the elements, which means that an accelerating voltage of the electron gun has to be higher than the elements of interest. However, to analyse elemental sulphur on the surface of the agglomerate, the accelerating voltage of the electron gun has to be higher than 2.307 kV because sulphur has a Kα of 2.307 kV (carbon = 0.277 kV, nitrogen = 0.392, and oxygen = 0.523 kV). This leads to two disadvantages. One is that long exposure times can lead to the sample burning. The second, and more important, is that the X-rays penetrate sub-surface layers. This implies that the EDX maps of the elements will be analysed from the surface and sub-surface layers of the precipitate.

2.8. X-ray diffraction

Samples were scanned using a Bruker D8 HRXRD. A PSD-LynxEye detector was used for acquiring the signals. All samples were in the form of a powder and placed on a silicon wafer. The scans were performed for 2θ between 5° and 70°, with a step of 0.04° and a scanning time of 5 s/step. The sample holder was rotating at 15° per scan. The emission gun had a Cu source with a characteristic wavelength of 1.5 Å. The electron gun was set to 40 kV and 20 mA. The baseline was subtracted from each scan.

2.9. XPS measurements

A PHI5000 VersaProbe III- Scanning XPS microprobe was utilised to study the samples. For the measurements a monochromatic Al source with an energy of 1486.6 eV and a beam size of 100 μm was applied. Dual charge compensation or argon ion gun (+ve) and electron neutraliser (-ve) were used because the samples were non-conductive. The system was aligned with $Au_4f_{7/2}$ (83.96 eV), $Ag_3d_{5/2}$ (368.18 eV) and $Cu_2p_{3/2}$ (932.62 eV) and the measurements with the sp2-hybridised carbon in graphene at 284.5 eV. Two scanning modes were used. The survey scan was performed from 0 to 1399 eV with a step size of 1.0 eV and a narrow scan was performed to study the chemical state of each element. The measurements were performed with a step size of 1.0 eV. Separate samples were prepared to study adsorbed asphaltene and adsorbed DBSA on GO. This was done to avoid signal overlap from asphaltene and DBSA because of the beam size. 4 samples were measured, i) GO, ii) GO deposited with DBSA, iii) GO deposited with asphaltenes, and iv) asphaltenes.

2.10. Experimental flowchart

The procedure of the sample preparation is shown in Fig. 1 as a flowchart. The different steps are: i). graphene is converted into graphene oxide ii). asphaltene is extracted from bitumen iii). asphaltene aggregates were produced from saturates, DBSA and asphaltenes, and iv). graphene oxide was introduced to asphaltene aggregates.

For the study, 6 characterization techniques were used (TLC-FID, FTIR, transmission light microscopy, SEM-EDX, XPS, and XRD) to obtain information about the parent material or the prepared samples. The motivations for utilizing the characterization techniques are presented

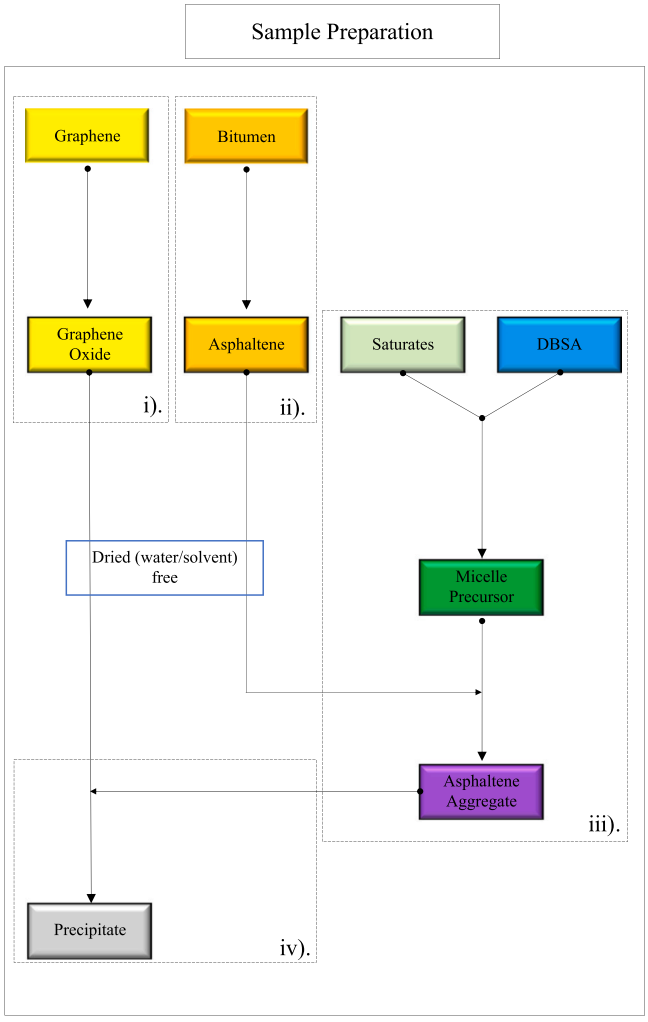

Fig. 1. A flow chart of the sample preparation. In the study, i). graphene was converted into graphene oxide, and ii). asphaltene was extracted from bitumen. Two samples were produced and used in this study iii) asphaltene aggregate and iv) asphaltene aggregate + graphene oxide.

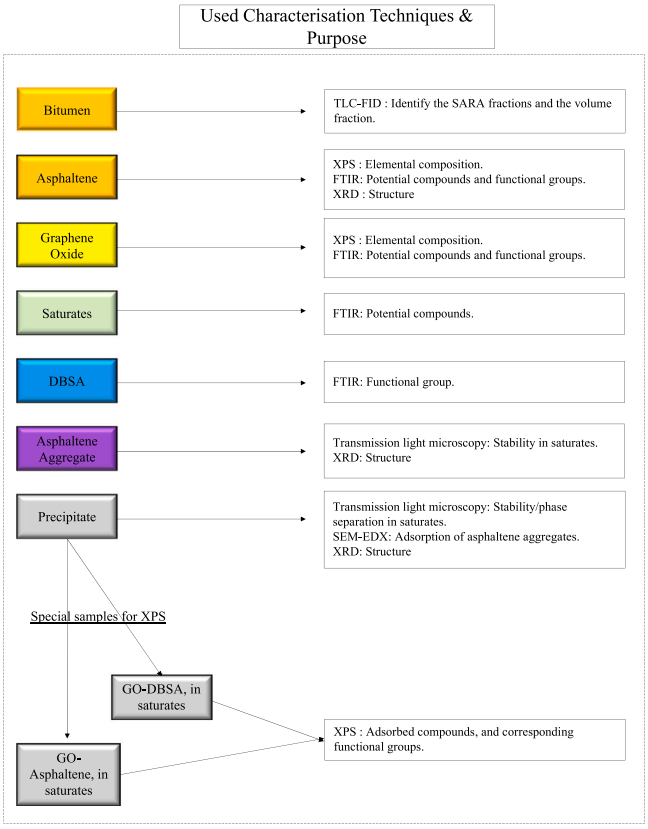

Fig. 2. A flow chart of the characterization techniques used in the work and the expected experimental outcome for each studied sample.

in Fig. 2.

3. Results

In order to verify the preparation procedure, the different components for the sample preparations (GO, DBSA, asphaltenes and saturates) were examined by Thin-layer chromatography (bitumen), ATR-FTIR (GO, DBSA, asphaltenes and saturates), and XPS (GO and asphaltenes). The results are shown in Figs. S1 (Thin-layer chromatography), S2 (FTIR), and Table S1 (XPS) in the Supplementary Information (SI). The results from the XPS measurements show (Table S1) the percentage of elements in GO and asphaltene. Furthermore, FTIR indicate that the functional groups present in asphaltene, DBSA and GO will play the most significant role in their interactions, as will be further discussed below.

3.1. Microscopic visualisation of the precipitate

Already a macroscopic visual inspection, shown in Fig. 3, indicates that an introduction of GO to an asphaltene aggregate system destabilises the structure of bitumen and causes immediate phase separation through the process of precipitation. From the examination of the asphaltene sample without GO, by transmission light microscope (Fig. 3a), it can be observed that for the asphaltene aggregate system, the image visualises a homogenous system with some small weak black dots or particles, which are assumed to be the asphaltene aggregates. Due to the size of these asphaltene aggregates, they were imaged using a polarised light filter. The asphaltene aggregates is the circular fringe pattern (ripples) in the image (Fig. 3a). The precipitated structure in the asphaltene aggregate system (after the introduction of GO) was also imaged, see Fig. 3d. These images were taken using phase contrast. In contrast to the observation of the sample without GO (Fig. 3a), large structures are now observed. These structures do not display any long-range order and can be seen to have a size distribution ranging from a few microns to up to 50 μm. The glowing ring around these structures is the boundary between the phase separated structure and saturates.

To check the stability of the particles found in the solvent phase of the precipitated sample (i.e., the asphaltene aggregate system after the introduction of GO), the samples was centrifuged (at 3500 rpm). From the images it is obvious that, in contrast to the sample with GO, which is completely precipitated (Fig. 3f), the sample with only asphaltene aggregate remained stable (Fig. 3c) This indicates that the particles found in the solvent phase of the asphaltene-GO sample (Fig. 3d) are less stable structures compared to that of asphaltenes without GO (Fig. 3a). It can therefore be stated that, after sufficiently long time, the particles will precipitate. Thus, already a macroscopic visual inspection strongly suggests that an introduction of GO to an asphaltene aggregate system destabilizes the structure of bitumen and causes immediate phase separation through the process of precipitation.

To get a deeper understanding of the nature of the precipitated structure seen in the lower panel of Figs. 3(d–f), i.e., the GO-asphaltene aggregates in the system, SEM imaging was conducted. From the results, shown in Fig. 4, it can be observed that the precipitated sample contains large agglomerated structures with smaller particles adsorbed on the surface, Figs. 4a. Fig. 4c shows that these particles, with a size of less than 100 nm, have a different contrast compared to the bulk of the agglomerate. Thus, from this initial observation, it can be predicted that the large agglomerated structures seen in Figs. 3d and 4 a are sheets of GO.

To verify these results an elemental analysis, by EDX, of the precipitate was performed. The results, which are shown in Fig. S3 of SI, reveal peaks for carbon, oxygen, sulphur, and nitrogen. This finding together with the results from ATR-FTIR of asphaltene (Figs. S2 of SI), which showed that nitrogen, oxygen and sulphur compounds are present in asphaltenes, is a strong indication on that the adsorbed particles are asphaltene. From Fig. S3 of SI, it can furthermore be observed that even if sulphur peaks are found profoundly on the particles adsorbed on the surface, they are also found throughout the surface of the agglomerates. The presence of sulphur on the entire agglomerate surface can be attributed to two primary sources, asphaltenes and DBSA. The uniform distribution of sulphur on the surface of the agglomerate is therefore most likely due to DBSA.

3.2. Surface analysis of particles adsorbed on the precipitate

To reach a deeper understanding of the molecular nature and the bonds formed by heteroatoms on the precipitate surface also XPS measurements were performed. The results are shown in Fig. 5, where Figs. 5a and d showing GO, Figs. 5b, e, g and h showing GO-asphaltene, and Figs. 5c, f and i showing GO-DBSA. From Fig. 5a there is a strong indication on that GO exists as a monolayer with a near proportion of sp2 hybridised carbon (peak1) and oxidised carbon species (peaks 2 and 3).

By comparing Figs. 5a and c it is obvious that after DBSA is added it is adsorbed on the surface of GO because of the appearance of a $\pi - \pi^*$ satellite (peak 2 in Fig. 5c). Moreover, it can be observed that oxidised carbon species are not visible in the spectrum of GO-DBSA (Figs. 5c and f). Instead, a doublet peak appears at 168.8 eV and 169.9 eV, for S_{2p} from the sulphonic group (peak 1 and 2 in Fig. 5i).

These features in the spectra indicate that DBSA adsorbs on the surface through the interaction with the delocalised electrons on GO and the donation of lone pair of electrons between the functional groups on GO and DBSA. The lack of oxidised carbon species (Figs. 5c and f) and the appearance of S_{2p} (peaks 1 and 2 in Fig. 5i) in the GO-DBSA spectra indicate that DBSA forms a uniform layer when adsorbed on the surface on GO. This is also the reason for why a uniform elemental sulphur spectrum is observed on the precipitate in the EDX analysis (Figs. S3 of SI). Furthermore, XPS is a surface technique that is efficient for up to 10 at. layers, therefore the lack of oxidised carbon species indicates that

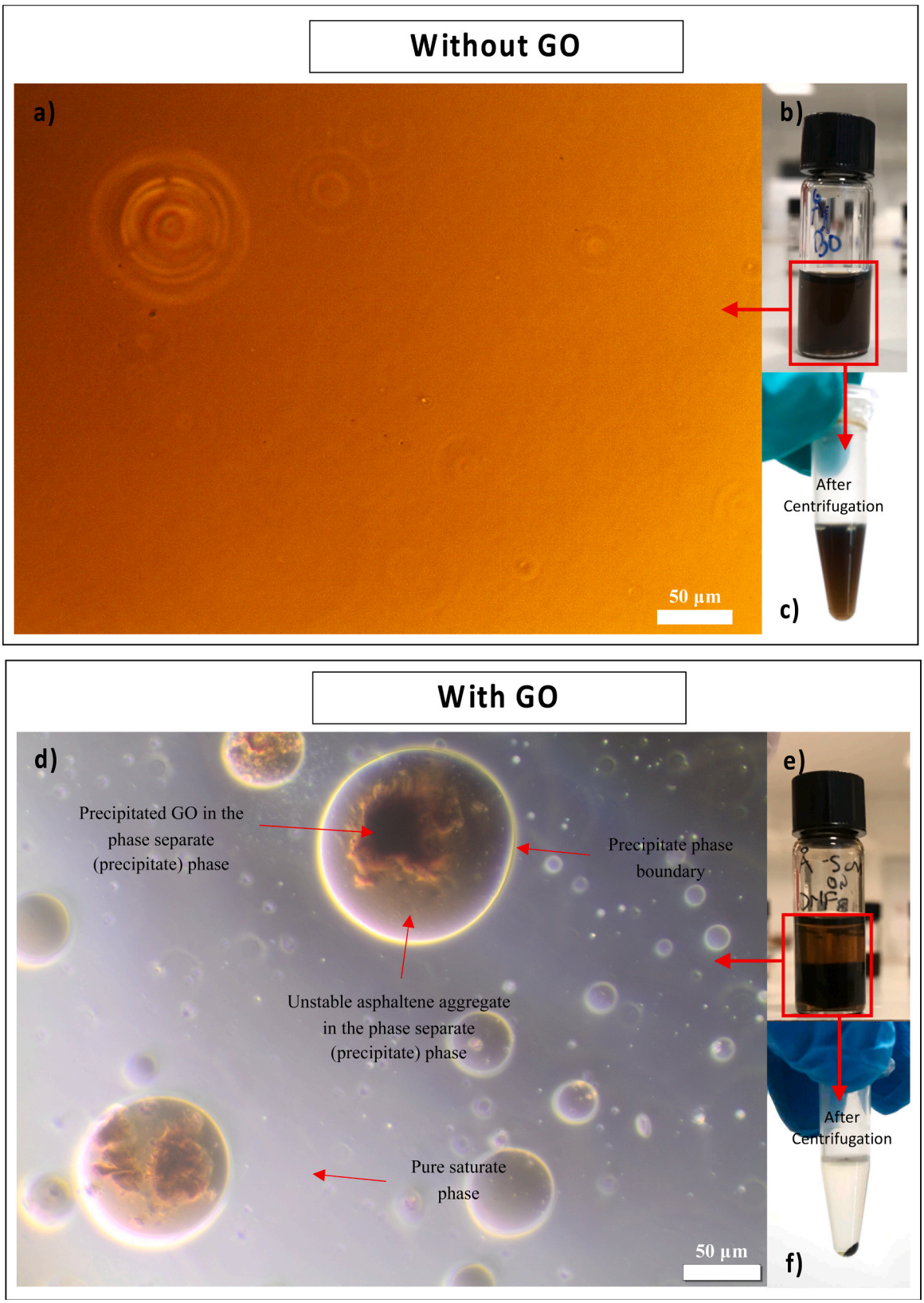

Fig. 3. Transmission light microscopy images of asphaltene aggregate and precipitate (asphaltene aggregate with GO). a) Asphaltene aggregates can be seen as the circular fringe pattern (ripples) in the image. Due to the size of the asphaltene aggregate, it was imaged using polarised light filter. b) Stable asphaltene nano-aggregate dispersed in micelle precursor. c) After centrifugation, asphaltene aggregates solution without GO were still stable. d) The precipitate (after the introduction of GO) was imaged under phase contrast. Large structures were observed. The glowing ring around the structures is the boundary between the phase separated structure and saturates. e) After introduction of GO to the asphaltene aggregate solution. f) After centrifugation, the precipitate in Fig. 2e and the suspension can be seen to completely precipitate.

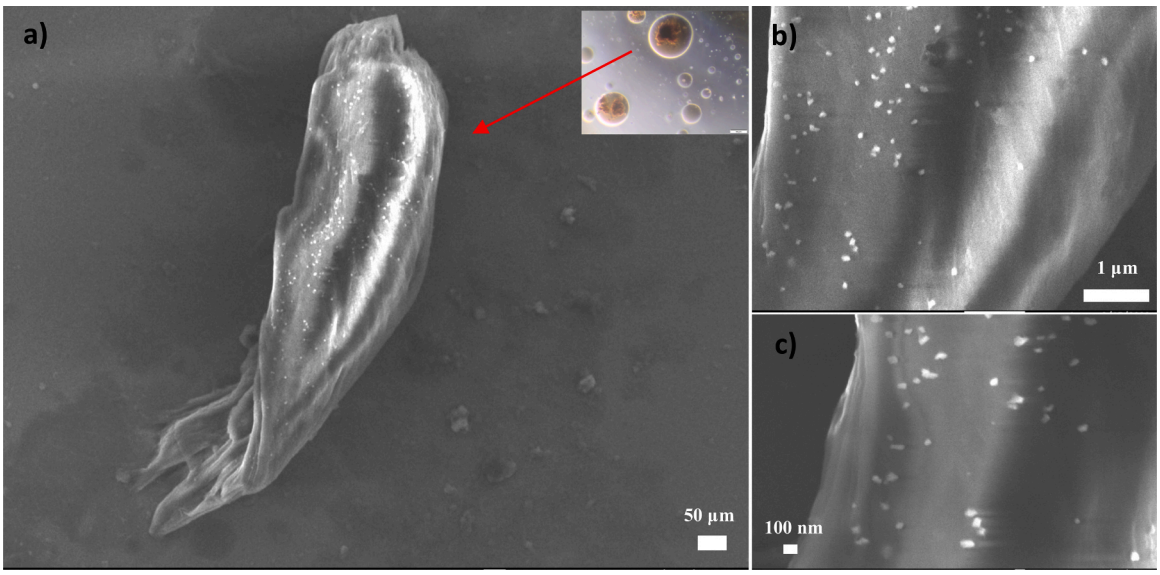

Fig. 4. a). SEM image of an agglomerated structure of the precipitate. Asphaltene nanoaggregates are seen to be adsorbed on the surface of GO. b & c). Zoomed in images of the agglomerate.

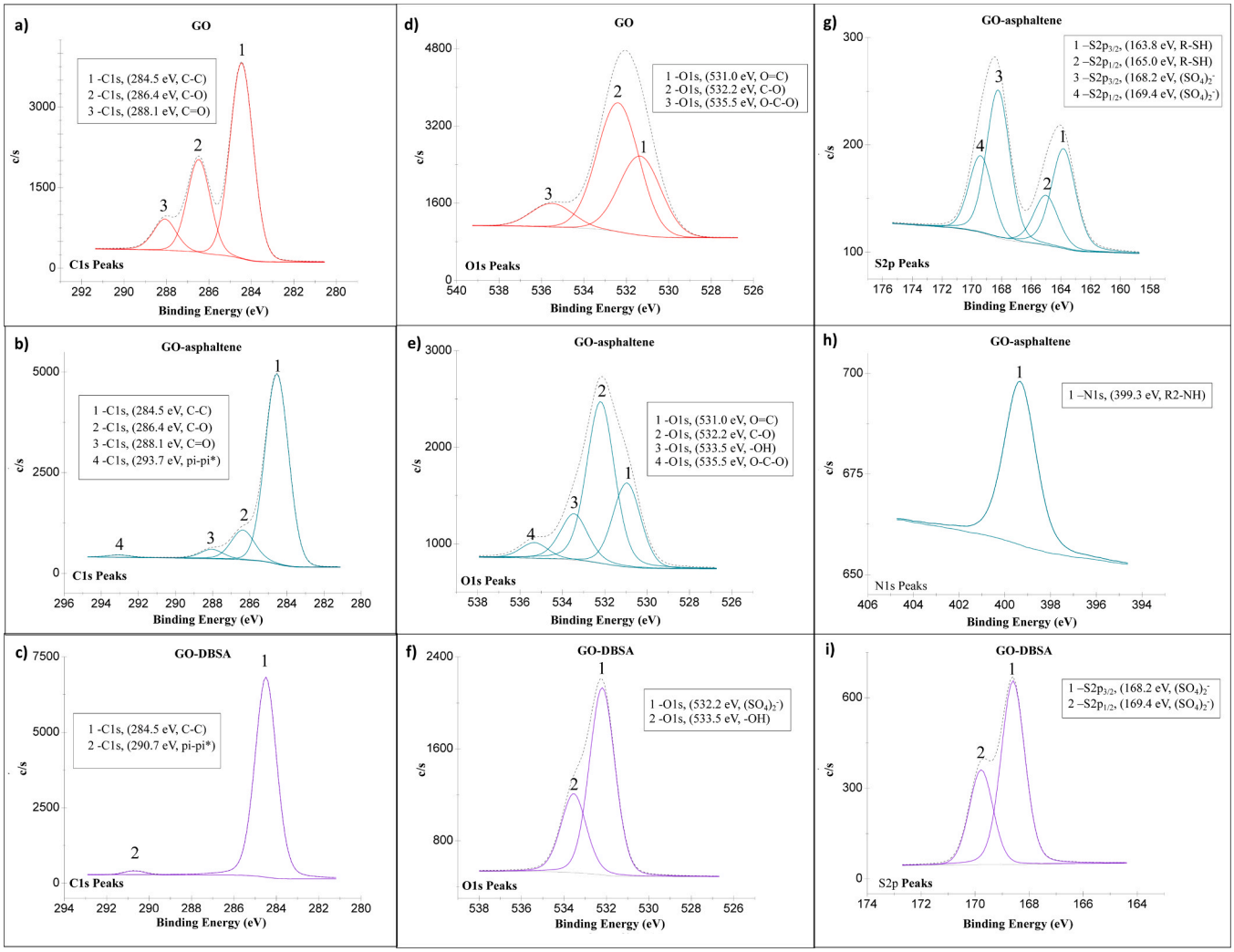

Fig. 5. The narrow scan results of the C1s (a, b, c), O1s (d, e, f), S_{2p} (g, i) and $N_{1\,s}$ (h) XPS spectra of C_{1S}: a) GO, b) GO-DBSA, and c) GO-asphaltene. XPS spectra of a $O_{1\,s}$: d) GO, e) GO-asphaltene, and f) GO-DBSA. XPS spectra of S_{2p}: g) GO-asphaltene and i) GO-DBSA. XPS spectrum of $N_{1\,s}$: h) GO-asphaltene.

the adsorbed DBSA is multi-layer thick (Figs. 5c and f).

From XPS it is also revealed that the spectral pattern of the adsorbed asphaltenes shows an atomic percentage of 74.2% carbon in the C_{1s} state (Table S1 in SI and Fig. 5b), which is a strong indication on that the adsorbed species are rich in carbon content. Further evaluation of the spectra also reveals the presence of multiple functional states of C, S, O and N (Figs. 5b, e, g and h). The spectra also show oxidised carbon species such as O-C═O and C–O (peaks 2 and 3 in Fig. 5b and peaks 1,2 and 4 in Fig. 5e). Similarly, a sulphonic group (peaks 3 and 4 in Fig. 5g), thiol (peaks 1 and 2 in Fig. 5g) and secondary amine (peak 1 in Fig. 5h) were also observed in the spectrum of GO-asphaltene. The observations of these functional groups are in coherence with the information obtained from the FTIR spectra of asphaltene nanoaggregates (see Fig. S2 in SI).

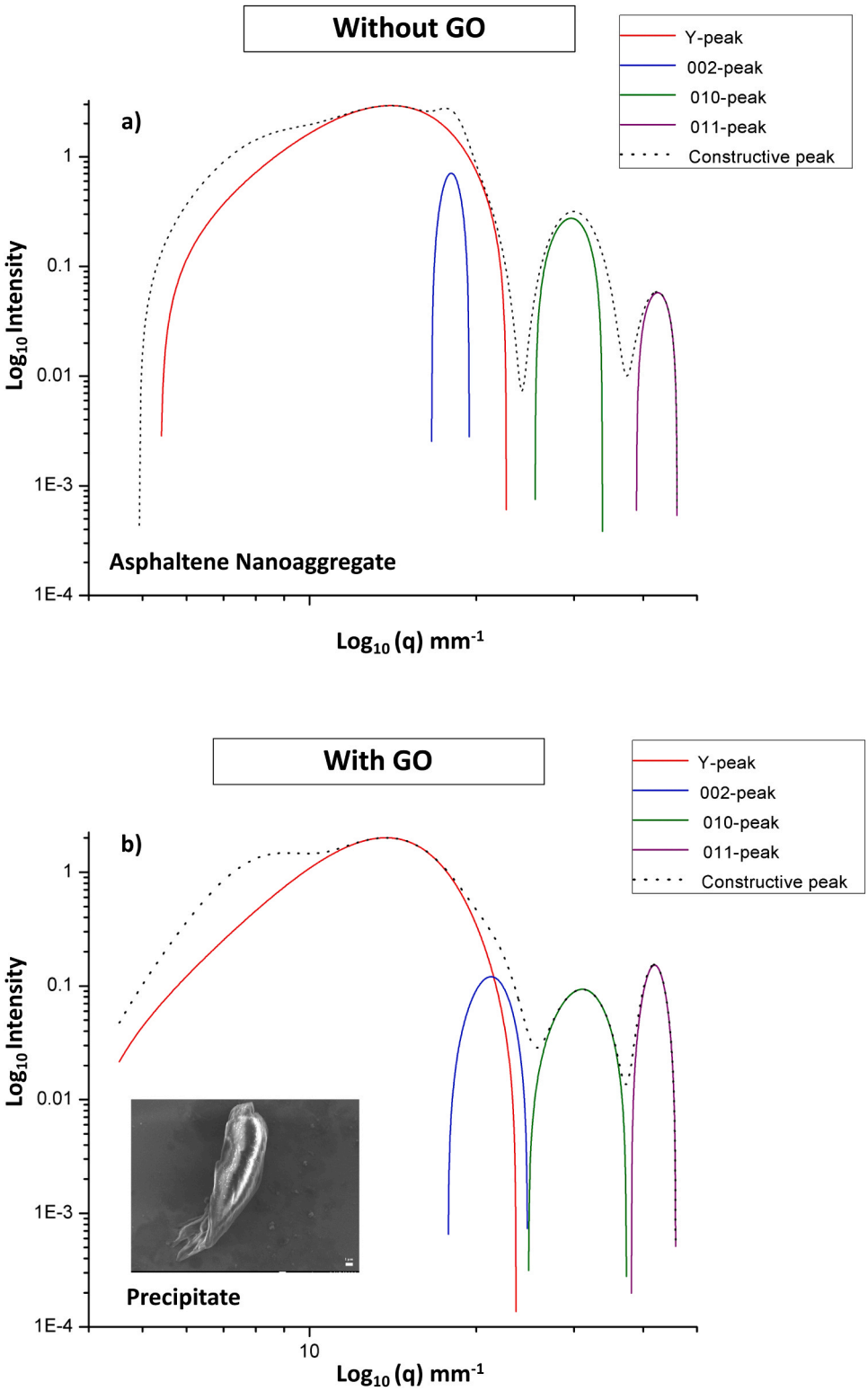

Fig. 6. In the figure a) shows the deconvoluted curve for asphaltenes and b) the deconvoluted curve for precipitate (agglomerated structure).

A $\pi - \pi^*$ satellite for the C_{1s} spectra of Fig. 5b is also observed, indicating that the adsorption mechanism of asphaltene on the surface of GO shows a similar interaction behaviour to DBSA (Figs. 5b and e). Also, the disappearance of sp2 carbon (Fig. 5b) and the appearance of heteroatomic functional groups (Figs. 5g and h) confirm that the adsorbed particles are asphaltene. Therefore, it can be concluded that both asphaltenes and DBSA are adsorbed on the surface of GO and that the particles observed by the SEM images (Fig. 4) on the precipitate are indeed destabilised asphaltene aggregates.

3.3. Structural evaluation of the precipitate

To further examine the structure of the precipitate shown in Fig. 4, also XRD was performed on the extracted asphaltene nanoaggregates and the precipitated structure. The result is shown in Fig. 6. For the analysis of the experimentally observed peaks we have used previous designations, where the peaks have been considered as quasi-Bragg-peaks caused by crystal-like local ordering [49]. Thus, despite that the true structure is amorphous, with only local structural ordering, as further evident from the lack of true Bragg-peaks in the experimental data, this quasi-crystalline designation has been used to describe the local crystal-like ordering. Thereby, the peaks shown in Fig. 6 have been deconvoluted with quasi-Bragg-peaks shown in the figure. Thereafter, Eqs. (1) to (5) were used to extract structural information from the curve fitting. In the Eqs. (1)–(3), q is defined as the momentum transfer, d is the real spacing and h, k and l are the Miller indices. The distances between the atoms in the assumed HCP-like (hexagonal closed packed) structure are determined by a and c (Eq. (2)).

$$q = \frac{2\pi}{\lambda} 2sin\Theta \tag{1}$$

$$\frac{1}{d_{002}} = \left[\frac{4}{3}\left(h^2 + k^2 + kh\right) + l^2\left(\frac{a}{c}\right)^2\right]^{\frac{1}{2}} \tag{2}$$

$$\frac{1}{d_{002}} = \frac{1}{2\pi q_{002}} \tag{3}$$

As shown in Fig. 6a (and Fig. S4 of SI for linear scales), the asphaltene nanoaggregates exhibit the expected characteristic peaks in XRD [64]. The positions and Full Width at Half Maximum (FWHM) of the different peaks are displayed in Table 1. As shown in the table, asphaltene nanoaggregates has a distinct graphitic peak for the 002 Miller plain, which is due to a relatively regular spacing between the aromatic layers. The 002 peak position can be used to calculate the Miller indices (Eqs. (2) and (3)) of the hexagonal close packing (HCP) carbon structures and is therefore used to identify the characteristic structure of asphaltene nanoaggregates [82].

Amongst the peaks, the γ-peak is caused by the aliphatic side chains in asphaltene nanoaggregates, see Fig. 6a. It can be noted that these side chains are also giving rise to the distinct alkyl C-H peak between 2800 cm^{-1} and 3000 cm^{-1} in the FTIR spectrum (Figs. S2 in SI). Using Bragg's law (Eq. (4)) and Scherrer crystallite equation (Eq. (5)), the aromatic nature of asphaltene nanoaggregates can be calculated, see Table 1. The 010-peak and the 011-peak in Fig. 6 provide information about the size and characteristics of the aromatic sheet.

From the position and width of the 002-peak it can be calculated, by Eq. (3), that there is a distance of 3.26 Å between the aromatic sheets in the asphaltene nanoaggregates, and a cluster diameter (L_c) of 14.3 Å (Eq. (4)).

$$L_c = \frac{0.45}{FWHM_{002}} \tag{4}$$

The cluster diameter is equivalent with the total thickness of each asphaltene nanoaggregate. Dividing the cluster diameter (L_C) by the spacing (d_M) between the aromatic sheets give that the asphaltene nanoaggregates used in this study have a thickness (M_e) of about 4 aromatic sheets (Eq. (5)).

$$M_c = \frac{L_c}{d_M} \tag{5}$$

The XRD data on the precipitate, indicates a substantial weakening and broadening of the 002-peak when GO is added, see Fig. 6b. The peak position corresponds to a calculated distance between the aromatic sheets of 2.98 Å, which is a value below the atomic distance between two carbon sheets. This observation together with the broadening of the 002-peak is a clear indication that the observed structure becomes more disordered, both locally and on a longer length-scale, and thereby even more amorphous in its nature.

From Fig. 6b another observable change is the decrease in the intensity of the γ-peak of the precipitate, which can also be associated with a loss of structural ordering. The GO sheets, onto which the asphaltene nanoaggregates are adsorbed, may increase the disorder of the asphaltene nanoaggregates and thereby result in a decrease of the intensity of the γ-peak. Furthermore, the intensity of the 011-peak is increased for the precipitate, in comparison with that of the pure asphaltene nanoaggregates, which often is associated with an increase in anisotropy. Therefore, this peak may be associated with a reordering of the GO sheets. Thus, the high aspect ratio combined with the precipitation can lead to such structural alterations.

4. Discussion

The XPS, XRD and SEM results, along with the visual inspection, confirm that GO interacts with the asphaltene aggregates in the system. The size of the deposited asphaltene nanoaggregates and the uniform layer of DBSA on GO are two interesting observations. It indicates that both asphaltene and DBSA adsorb on the surface of GO. However, the DBSA molecules prefer to adsorb on GO over the asphaltene nanoaggregates. Without DBSA to stabilise, the asphaltene nanoaggregates self-assembly to form larger structures. These large asphaltene structures (i.e., the small, adsorbed particles in Fig. 4) will then adsorb on the surface of GO. A schematic illustration of this scenario is shown in Fig. 7.

Table 1
Values obtained from the XRD analysis. The table displays the FWHM and the peak position of the gamma peak, the 002-peak, the 010-peak and the 001-peak of both the asphaltene nanoaggregates and precipitate. The margin for error in the XRD measurements for asphaltenes is comparatively less prominent when compared to potential variations in sample data (asphaltenes) due to the possible discrepancy in the chemical characteristics of asphaltene from source to source. Due to this, an error margin of 10% can be accounted for in the data presented in the table.

Peak	FWHM (q) $_{asphaltene\ nanoaggregates}$	Peak position (q) $_{asphaltene\ nanoaggregates}$	Peak Intensity $_{asphaltene\ nanoaggregates}$	FWHM (q) $_{precipitate}$	Peak Position (q) $_{precipitate}$	Peak Intensity $_{precipitate}$
ɣ-peak	9.35	14.02	3.23	7.99	13.74	2.04
002-peak	2.13	18.10	1.01	4.57	21.26	0.15
010-peak	8.54	29.64	0.58	8.77	31.07	0.12
011-peak	14.30	42.46	0.36	4.77	41.92	0.18

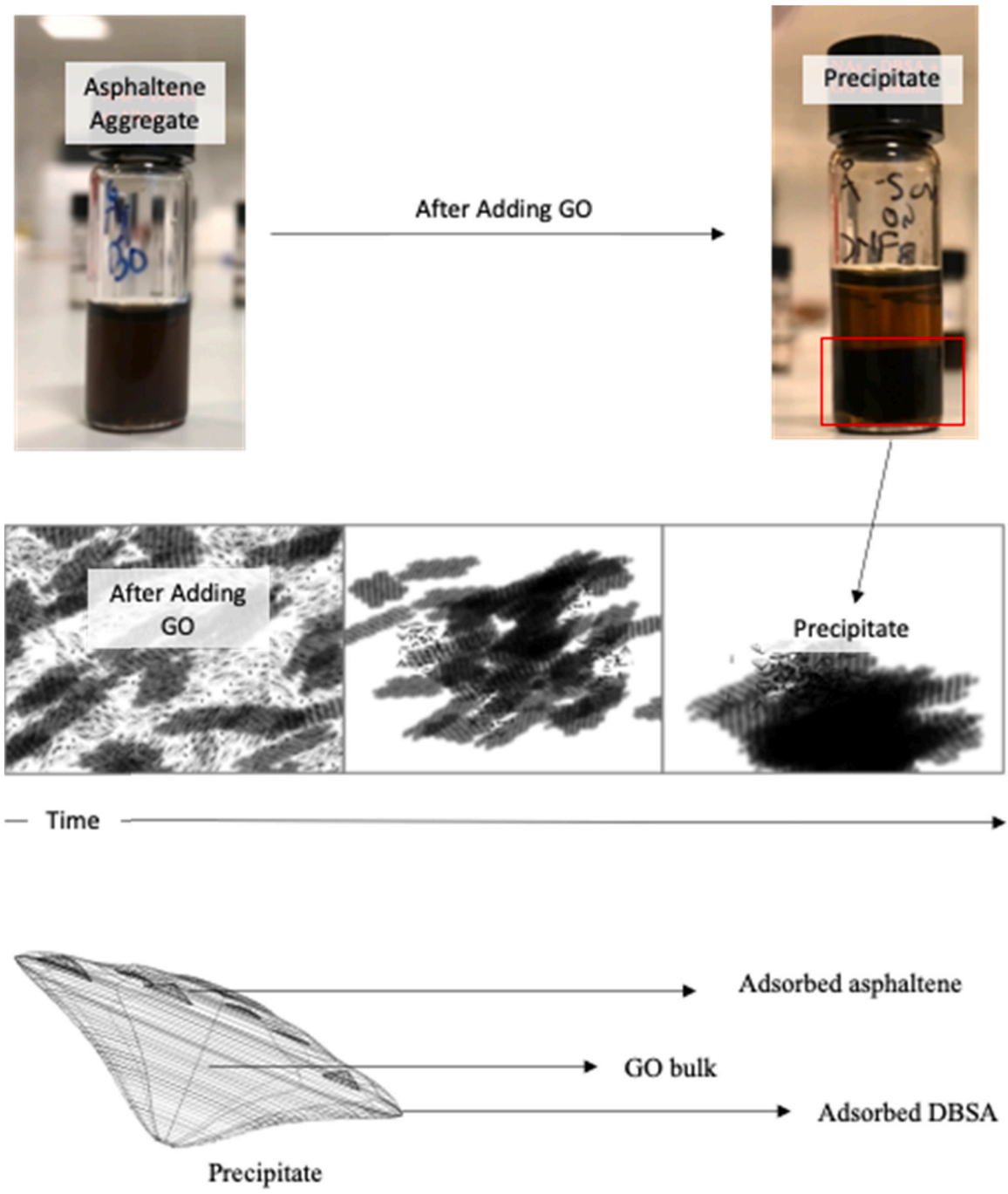

Fig. 7. From left to right: the stable asphaltene dispersed in the micelle precursor, after introduction of GO to the asphaltene aggregate solution. Asphaltene aggregates are stable while the sample in which GO is added has precipitated. In addition, an illustration of the precipitated structure and the mechanism of destabilisation and precipitation.

From the results, it can be concluded that if GO is added to crude oil or crude derivatives such as bitumen, the polyaromatic hydrocarbons (PAHs) will be adsorbed on the surface of GO and the structure of asphaltene containing materials such as bitumen will be lost. Depending on the viscosity and temperature, this could be observed as a phase separation or local agglomeration [1].

In the absence of GO, the driving force for structural stability between asphaltenes and DBSA comes from the interaction between the carboxylic group found on asphaltenes and the sulfoxide group on DBSA [49–65]. With the introduction of GO, DBSA and asphaltenes will prefer to accept electrons from GO by forming bonds directly with the electron-rich functional groups on GO and not between asphaltene and DBSA.

In general, polymers and small PAHs have been shown to adsorb on the surface of pristine graphene [79,80]. Adsorption of small PAHs on large graphitic surfaces occurs by offset with the base plane, though non-covalent interaction [79,80]. In such an interaction, the π orbitals of GO interacts with the delocalised electrons on PAH structures, such as asphaltenes, to form $\pi - \pi$ system. This interaction will become stronger if one of the species donates a lone-pair electron to the antibonding orbitals of the other, as in the case of the GO-asphaltene sample, due to the functional groups present on GO and asphaltene. As observed by FTIR and XPS, GO contains functional groups such as hydroxyl and ketones, which both are good electron donors. Strong acid groups such

as sulfonic acid and carboxylic acid have high electron affinity, meaning that the acidic head of DBSA and acid functional groups on asphaltene can obtain electrons from GO. This occurs through hydrogen bonding, electrostatic interaction, hydrophobic interaction, and ion bridging between GO, asphaltene and DBSA. By this mechanism, asphaltene and DBSA will be able to form layers on top of GO, through the spontaneous ordering of the molecules at the interface with GO. The observations from XPS and SEM confirm this argument. Therefore, the mechanism that causes the GO induced phase separation of the asphaltene aggregate system is a complex and multistage process, that involves both removal and re-engagement of bonds. This finding is critical for the understanding of the behaviour of asphaltene in bitumen, and thereby also the properties of bitumen, which to a large extent are lost by the introduction of GO and the associated phase separation.

Bitumen is dominantly used to construct roads. Most often, bitumen is heated to temperatures such as 180 °C [1] to reduce its viscosity to make it suitable for transportation. An alternative to heating is emulsification [32–37]. However, as mentioned in the introduction, asphaltenes contribute to the stabilisation of water-in-oil/water-in-bitumen emulsions by interacting with water at the interface [32]. From this study, which is focused on the influence of GO on a pure water-free/oil-based asphaltenes aggregate system, it is evident that using GO as an emulsifying agent will cause the asphaltenes in a bitumen emulsion to be adsorbed on the GO surface. Thus, one finding from this study implies that the demulsified bitumen will contain irreversible forms of the structure shown in Figs. 3d–f, instead of the expected asphaltene aggregates (Figs. 3a–c).

The irreversibility of the precipitated structure was further confirmed by repeated sonication and centrifugation. Another finding from this study is therefore an indication on that the agglomerated structure is detrimental, i.e., it causes a phase separation in which bitumen loses its asphaltenes and resins. This will directly influence the structure and function of bitumen, and consequently, cause significant industrial and commercial losses. For example, while the surface of asphaltene aggregates is phase compatible with the saturates and aromatics present in bitumen, the present results show that the surface of the agglomerated structure is not. Thus, an effect like in the case of blending immiscible polymers [81]. So, when the material is under tribological loading or during long term aging, the surface of roads will be more prone to dislodging and forming particulate matter [82,83]. These particles can enter air, water or soil to cause detrimental environmental impact [84].

When GO is added to bitumen and the temperature is increased the characteristic viscosity of bitumen is lost and the agglomerates undergo an irreversible phase separation followed by precipitation, see Figs. 4d–f. Thus, unlike the asphaltene aggregates, the agglomerate phase will remain phase separated even after the heat is lowered. This is a most critical effect as it causes bitumen to lose its characteristic properties because the asphaltenes and resins will remain adsorbed on the phase separated agglomerates.

It is well-known that nanoparticles have a high aspect ratio and when they are introduced in large volumes, they will cause a dominance in the influence of a material, like the solid phase of bitumen. By incorporating large volumes of nanoparticles, the solid phase is thus expected to increase [66–77]. By using characterisation methods focused on macroscopic properties of the bulk material, e.g., the complete nanomodified bitumen, the pseudo influence of the nanoparticles, such as saturates and asphaltenes (which are of much larger size), might be masked. This, in turn, results in that information about any microscopic structural changes are overlooked. Thus, the nanomodified bitumen appears to have undergone a structural and functional enhancement. Therefore, the results found in the literature showing improvement of bitumen is possible a misinterpretation of the results. A third important fining is therefore that earlier reported improvements of the material properties of bitumen by incorporating GO, can be interpreted as false positive [66–77]. This can either be a consequence of the nature of the bitumen studied or, most likely, due to the characterisation techniques used to study the influence of modifiers on bitumen, such as dynamic shear rheometer for viscoelastic changes and infrared photography for heat flow through bitumen, which all measures more macroscopic properties.

5. Conclusions

This study is the first with the focus on determining how the structural stability of asphaltene aggregates is affected by the introduction of nanoparticles, especially GO, with the goal to understand the impact of using GO as a demulsification agent of bitumen-water emulsion, and its subsequent impact on the function of bitumen, post demulsification. By use of different experimental techniques, we were able to observe that the destabilisation effect by introducing GO to asphaltene aggregate was immediate, and that the destabilisation was followed by a phase separation with a precipitation as a consequence.

From the result obtained by XRD it was concluded that the precipitated structure becomes more disordered, both locally and on longer length-scales, i.e., the structure becomes even more amorphous in its nature. The precipitate characterisation by SEM-EDX and XPS show that asphaltene and DBSA are adsorbed on the surface of GO, and that the oxygen functional groups present on the surface of GO causes the adsorption of asphaltene and DBSA. This in turn, causes a clustering of the polar components.

Thus, the results from this study show that nanoparticles, such as graphene or GO, in the natural form are unfavourable to be used as demulsification agents or material-enhancing agents for bitumen. This is because they interact with asphaltenes through hydrogen bonds, $\pi - \pi$ interactions and acid-base interactions.

Funding sources

The research was funded by the Norwegian Public Road Administration.

CRediT authorship contribution statement

Govindan Induchoodan: Conceptualization, Methodology, Validation, Writing – original draft. **Helen Jansson:** Supervisor, Validation, Writing – original draft. **Jan Swenson:** Supervisor, Validation, Writing – original draft.

Declaration of Competing Interest

The authors do not claim any conflict-of-interest.

Acknowledgements

The authors of this paper would like to thank Norwegian Public Road Administration (NPRA) Project ID: 2011 067932 for funding this research. The authors would also like to thank Amir Saeid Mohammadi, Ezio Zanghellini for support in performing the experiments.

Author contributions

The manuscript was written through contributions of all authors. All authors have given approval to the final version of the manuscript.

Appendix A. Supporting information

Supplementary data associated with this article can be found in the online version at doi:10.1016/j.colsurfa.2021.127614.

References

[1] D. Petrauskas, S. Ullah. Manufacture and Storage of Bitumen, Shell Handbook, Sixth ed., Shell Bitumen, 2015.
[2] M. Kaiser, A. Klerk, J. Gary, G. Handwerk. Introduction (chapter), Petroleum Refining, fifth ed., Technology and Economics, 2007, pp. 1–40.
[3] O. Mullins, The modified yen model†, Energy Fuels 24 (4) (2010) 2179–2207.
[4] S. Ashoori, M. Sharifi, M. Masoumi, M. Mohammad Salehi, The relationship between SARA fractions and crude oil stability, Egypt. J. Pet. 26 (1) (2017) 209–213.
[5] L. Chen, A. Bertolini, F. Dubost, V. Achourov, S. Betancourt, J. Cañas, H. Dumont, A. Pomerantz, O. Mullins, Yen–mullins model applies to oilfield reservoirs, Energy Fuels 34 (2020) 14074–14093.
[6] M.H. Schneider, A.B. Andrews, S. Mitra-Kirtley, O.C. Mullins, Asphaltene molecular size by fluorescence correlation spectroscopy, Energy Fuels 21 (2007) 2875–2882.
[7] R.E. Guerra, K. Ladavac, A.B. Andrews, O.C. Mullins, P.N. Sen, Diffusivity of coal and petroleum asphaltene monomers by fluorescence correlation spectroscopy, Fuel 86 (2007) 2016–2020.
[8] N.V. Lisitza, D.E. Freed, P.N. Sen, Y.-Q. Song, Study of asphaltene nanoaggregation by nuclear magnetic resonance (NMR), Energy Fuels 23 (2009) 1189–1193.
[9] A.R. Hortal, B. Martínez-Haya, M.D. Lobato, J.M. Pedrosa, S. Lago, On the determination of molecular weight distributions of asphaltenes and the aggregates in laser desorption ionization experiments, J. Mass Spectrom. 41 (2006) 960–968.
[10] R.P. Rodgers, A.G. Marshall, Petroleomics: advanced characterization of petroleum-derived materials by Fourier transform ion cyclotron resonance mass spectrometry (FT-ICR MS), in: O.C. Mullins, E.Y. Sheu, A. Hammami, A.G. Marshall (Eds.), Asphaltenes, Heavy Oils, and Petroleomics, Springer, New York, 2007, pp. 63–93, https://doi.org/10.1007/0-387-68903-6_3.
[11] A.G. Marshall, R.P. Rodgers, Petroleomics: chemistry of the underworld, Proc. Natl. Acad. Sci. U.S.A. 105 (47) (2008) 18090–18095.
[12] (a) T. Glattke, M. Chacón-Patiño, A. Marshall, R. Rodgers, Molecular characterization of photochemically produced asphaltenes via photooxidation of deasphalted crude oils, Energy Fuels 34 (2020) 14419–14428;
(b) B.; Schuler, G.; Meyer, D.; Pena, O.C.; Mullins, L. Gross, Unraveling the molecular structures of asphaltenes by atomic force microscopy, J. Am. Chem. Soc. 137 (31) (2015) 9870–9876.
[13] B. Schuler, S. Fatayer, G. Meyer, E. Rogel, M. Moir, Y. Zhang, M.R. Harper, A. E. Pomerantz, K.D. Bake, M. Witt, D. Peña, J.D. Kushnerick, O.C. Mullins, C. Ovalles, F.G.A. van den Berg, L. Gross, Heavy oil based mixtures of different origins and treatments studied by atomic force microscopy, Energy Fuels 31 (7) (2017) 6856–6861.
[14] F. Handle, M. Harir, J. Füssl, A. Koyun, D. Grossegger, N. Hertkorn, L. Eberhardsteiner, B. Hofko, M. Hospodka, R. Blab, P. Schmitt-Kopplin, H. Grothe, Tracking aging of bitumen and its saturate, aromatic, resin, and asphaltene fractions using high-field fourier transform ion cyclotron resonance mass spectrometry, Energy Fuels 31 (5) (2017) 4771–4779.
[15] W. A. Abdallah, Y. Yang, Raman spectrum of asphaltene, Energy Fuel 26 (11) (2012) 6888–6896.
[16] K. Bake, P. Craddock, T. Bolin, W. Abdallah, S. Mitra-Kirtley, A. Andrews, O. Mullins, A. Pomerantz, Structure-solubility relationships in coal, petroleum, and immature source-rock-derived asphaltenes, Energy Fuels 34 (9) (2020) 10825–10836.
[17] J. Putman, R. Moulian, C. Barrère-Mangote, R. Rodgers, B. Bouyssiere, P. Giusti, A. Marshall, Probing aggregation tendencies in asphaltenes by gel permeation chromatography. Part 1: online inductively coupled plasma mass spectrometry and offline fourier transform ion cyclotron resonance mass spectrometry, Energy Fuels 34 (7) (2020) 8308–8315.
[18] J. Putman, R. Moulian, D. Smith, C. Weisbrod, M. Chacón-Patiño, Y. Corilo, G. Blakney, L. Rumancik, C. Barrère-Mangote, R. Rodgers, P. Giusti, A. Marshall, B. Bouyssière, Probing aggregation tendencies in asphaltenes by gel permeation chromatography. Part 2: online detection by fourier transform ion cyclotron resonance mass spectrometry and inductively coupled plasma mass spectrometry, Energy Fuels 34 (9) (2020) 10915–10925.
[19] M. Asemani, A. Rabbani, Detailed FTIR spectroscopy characterization of crude oil extracted asphaltenes: curve resolve of overlapping bands, J. Pet. Sci. Eng. 185 (2020), 106618.
[20] Y. Ruiz-Morales, O. Mullins, Polycyclic aromatic hydrocarbons of asphaltenes analyzed by molecular orbital calculations with optical spectroscopy, Energy Fuels 21 (1) (2007) 256–265.
[21] J. Eyssautier, P. Levitz, D. Espinat, J. Jestin, J. Gummel, I. Grillo, L. Barre, Insight into asphaltene nanoaggregate structure inferred by small angle neutron and X-ray scattering, J. Phys. Chem. B 115 (21) (2011) 6827–6837.
[22] J. Eyssautier, I.; Hénaut, P.; Levitz, D.; Espinat, L. Barré, Organization of asphaltenes in a vacuum residue: a small-angle xray scattering (SAXS)−viscosity approach at high temperatures, Energy Fuels 26 (5) (2012) 2696–2704.
[23] G. Andreatta, N. Bostrom, O.C. Mullins, High-Q ultrasonic determination of the critical nanoaggregate concentration of asphaltenes and the critical micelle concentration of standard surfactants, Langmuir 21 (2005) 2728–2736.
[24] G. Andreatta, C.C. Goncalves, G. Buffin, N. Bostrom, C.M. Quintella, F. Arteaga-Larios, E.; Pérez, O.C. Mullins, Nanoaggregates and structure- function relations in asphaltenes, Energy Fuels 19 (4) (2005) 1282–1289.
[25] H. Zeng, Y.-Q. Song, D.L. Johnson, O.C. Mullins, Critical nanoaggregate concentration of asphaltenes by direct-current (DC) eletrical conductivity, Energy Fuels 23 (2009) 1201–1208.
[26] L. Goual, M. Sedghi, H. Zeng, F. Mostowfi, R. McFarlane, O.C. Mullins, On the formation and properties of asphaltene nanoaggregates and clusters by DC-conductivity and centrifugation, Fuel 90 (7) (2011) 2480–2490.
[27] L. Goual, M. Sedghi, F. Mostowfi, R. McFarlane, A.E. Pomerantz, S. Saraji, O. C. Mullins, Cluster of asphaltene nanoaggregates by DC conductivity and centrifugation, Energy Fuels 28 (8) (2014) 5002–5013.
[28] M. Anisimov, I. Yudin, V. Nikitin, G. Nikolaenko, A. Chernoutsan, H. Toulhoat, D. Frot, Y. Briolant, Asphaltene aggregation in hydrocarbon solutions studied by photon correlation spectroscopy, J. Phys. Chem. 99 (23) (1995) 9576–9580.
[29] R. Xiong, J. Guo, W. Kiyingi, H. Feng, T. Sun, X. Yang, Q. Li, Method for judging the stability of asphaltenes in crude oil, Omega 5 (34) (2020) 21420–21427.
[30] M. Nategh, H. Mahdiyar, M. Malayeri, M. Binazadeh, Impact of asphaltene surface energy on stability of asphaltene–toluene system: a parametric study, Langmuir 34 (46) (2018) 13845–13854.
[31] D. Lesueur, The colloidal structure of bitumen: consequences on the rheology and on the mechanisms of bitumen modification, Adv. Colloid Interface Sci. 145 (1–2) (2009) 42–82.
[32] S. Gorbacheva, S. Ilyin, Structure, rheology and possible application of water-in-oil emulsions stabilized by asphaltenes, Colloids Surf. A Physicochem. Eng. Asp. 618 (2021), 126442.
[33] F.; Mahmoudi Alemi, S.; Mousavi Dehghani, A.; Rashidi, N.; Hosseinpour, S. Mohammadi, Synthesize of MWCNT-Fe2o3 nanocomposite for controlling formation and growth of asphaltene particles in unstable crude oil, Colloids Surf. A Physicochem. Eng. Asp. 615 (2021), 126295.
[34] D. Simionesie, G. O'Callaghan, J. Costa, L. Giusti, W. Kerr, J. Sefcik, P. Mulheran, Z. Zhang, Clustering behaviour of polyaromatic compounds mimicking natural asphaltenes, Colloids Surf. A Physicochem. Eng. Asp. 603 (2020), 125221.
[35] S. Xia, K. Kostarelos, The charge alteration of asphaltenes during electro-deposition, Colloids Surf. A Physicochem. Eng. Asp. 598 (2020), 124808.
[36] A. Piroozian, M. Hemmati, M. Safari, A. Rahimi, O. Rahmani, S. Aminpour, A. Pour, A mechanistic understanding of the water-in-heavy oil emulsion viscosity variation: effect of asphaltene and wax migration, Colloids Surf. A Physicochem. Eng. Asp. 608 (2021), 125604.
[37] A. Cagna, G. Esposito, A. Quinquis, D. Langevin, On the reversibility of asphaltene adsorption at oil-water interfaces, Colloids Surf. A Physicochem. Eng. Asp. 548 (2018) 46–53.
[38] H. Wang, J. Liu, H. Xu, Z. Ma, W. Jia, S. Ren, Demulsification of heavy oil-in-water emulsions by reduced graphene oxide nanosheets, RSC Adv. 6 (108) (2016) 106297–106307.
[39] J. Liu, H. Wang, X. Li, W. Jia, Y. Zhao, S. Ren, Recyclable magnetic graphene oxide for rapid and efficient demulsification of crude oil-in-water emulsion, Fuel 189 (1) (2017) 79–87.
[40] T. Lan, H. Zeng, T. Tang, Molecular dynamics study on the mechanism of graphene oxide to destabilize oil/water emulsion, J. Phys. Chem. C. 123 (37) (2019) 22989–22999.
[41] J. Liu, X. Li, W. Jia, Z. Li, Y. Zhao, S. Ren, Demulsification of crude oil-in-water emulsions driven by graphene oxide nanosheets, Energy Fuels 29 (7) (2015) 4644–4653.
[42] F. Ye, X. Jiang, Y. Mi, J. Kuang, Z. Huang, F. Yu, Z. Zhang, H. Yuan, Preparation of oxidized carbon black grafted with nanoscale silica and its demulsification performance in water-in-oil emulsion, Colloids Surf. A Physicochem. Eng. Asp. 582 (5) (2019), 123878.
[43] H. Xu, W. Jia, S. Ren, J. Wang, S. Yang, Stable and efficient demulsifier of functional fluorinated graphene for oil separation from emulsified oily wastewaters, J. Taiwan Inst. Chem. Eng. 93 (2018) 492–499.
[44] D. Arab, A. Kantzas, S. Bryant, Nanoparticle stabilized oil in water emulsions: a critical review, J. Pet. Sci. Eng. 163 (2018) 217–242.
[45] H. Son, H. Kim, G. Lee, J. Kim, W. Sung, Enhanced oil recovery using nanoparticle-stabilized oil/water emulsions, Korean J. Chem. Eng. 31 (2013) 338–342.
[46] I. Gavrielatos, R. Dabirian, R. Mohan, O. Shoham, Oil/water emulsions stabilized by nanoparticles of different wettabilities, J. Fluids Eng. (2018) 141.
[47] F. Goodarzi, S. Zendehboudi, A comprehensive review on emulsions and emulsion stability in chemical and energy industries, Can. J. Chem. Eng. 97 (1) (2018) 281–309.
[48] A. Dimiev, S. Eigler. Graphene Oxide, first ed., John Wiley & Sons, Ltd., New York, 2016, pp. 36–84.
[49] L. Goual, A. Firoozabadi, Effect of resins and DBSA on asphaltene precipitation from petroleum fluids, AIChE J. 50 (2) (2004) 470–479.
[50] C. Chang, H. Fogler, Stabilization of asphaltenes in aliphatic solvents using alkylbenzene-derived amphiphiles. 1. Effect of the chemical structure of amphiphiles on asphaltene stabilization, Langmuir 10 (6) (1994) 1749–1757.
[51] L. Goual, M. Sedghi, Role of ion-pair interactions on asphaltene stabilization by alkylbenzenesulfonic acids, J. Colloid Interface Sci. 440 (2015) 23–31.
[52] S. Fakher, M. Ahdaya, M. Elturki, A. Imqam, Critical review of asphaltene properties and factors impacting its stability in crude oil, J. Pet. Explor. Prod. Technol. 10 (3) (2019) 1183–1200.
[53] Y. Larichev, A. Nartova, O. Martyanov, The influence of different organic solvents on the size and shape of asphaltene aggregates studied via small-angle X-ray scattering and scanning tunneling microscopy, Adsorpt. Sci. Technol. 34 (2–3) (2016) 244–257.
[54] G. González, A. Middea, Peptization of asphaltene by various oil soluble amphiphiles, Colloids Surf. 52 (1991) 207–217.
[55] O. Mullins, Review of the molecular structure and aggregation of asphaltenes and petroleomics, SPE J. 13 (01) (2008) 48–57.

[56] Speight, J. Asphaltenes: Fundamentals And Applications By E. Y. Sheu And O. C. Mullins. Plenum Press, New York, 1995; 236 Pages Plus Index. ISBN No. 0–306-45191–3. Energy & Fuels 1996, 10 (6), 1282–1282.
[57] H. Santos Silva, A. Alfarra, G. Vallverdu, D. Bégué, B. Bouyssiere, I. Baraille, Impact of h-bonds and porphyrins on asphaltene aggregation as revealed by molecular dynamics simulations, Energy Fuels 32 (11) (2018) 11153–11164.
[58] H. Pan, A. Firoozabadi, Thermodynamic micellization model for asphaltene precipitation inhibition, AIChE J. 46 (2) (2000) 416–426.
[59] R. Skartlien, S. Simon, J. Sjöblom, A DPD study of asphaltene aggregation: the role of inhibitor and asphaltene structure in diffusion-limited aggregation, J. Dispers. Sci. Technol. 38 (3) (2016) 440–450.
[60] S. Hashmi, K. Zhong, A. Firoozabadi, Acid–base chemistry enables reversible colloid-to-solution transition of asphaltenes in non-polar systems, Soft Matter 8 (33) (2012) 8778.
[61] C. Chang, H. Fogler, Stabilization of asphaltenes in aliphatic solvents using alkylbenzene-derived amphiphiles. 1. Effect of the chemical structure of amphiphiles on asphaltene stabilization, Langmuir 10 (6) (1994) 1749–1757.
[62] B. Jiang, R. Zhang, N. Yang, L. Zhang, Y. Sun, C. Jian, L. Liu, Z. Xu, Molecular mechanisms of suppressing asphaltene aggregation and flocculation by dodecylbenzenesulfonic acid probed by molecular dynamics simulations, Energy Fuels 33 (6) (2019) 5067–5080.
[63] T. Al-Sahhaf, M. Fahim, A. Elkilani, Retardation of asphaltene precipitation by addition of toluene, resins, deasphalted oil and surfactants, Fluid Phase Equilibr. 194–197 (2002) 1045–1057.
[64] M. Alhreez, D. Wen, Molecular structure characterization of asphaltene in the presence of inhibitors with nanoemulsions, RSC Adv. 9 (34) (2019) 19560–19570.
[65] T. Chew, R. Daik, M. Hamid, Thermal conductivity and specific heat capacity of dodecylbenzenesulfonic acid-doped polyaniline particles—water based nanofluid, Polymers 7 (7) (2015) 1221–1231.
[66] S. Jahromi, A. Khodaii, Effects of nanoclay on rheological properties of bitumen binder, Constr. Build. Mater. 23 (8) (2009) 2894–2904.
[67] H. Yao, Q. Dai, Z. You, M. Ye, Y. Yap, Rheological properties, low-temperature cracking resistance, and optical performance of exfoliated graphite nanoplatelets modified asphalt binder, Constr. Build. Mater. 113 (2016) 988–996.
[68] N. Habib, N. Aun, S. Zoorob, P. Lee, Use of graphene oxide as a bitumen modifier: an innovative process optimization study, Adv. Mater. Res. 1105 (2015) 365–369.
[69] J. Crucho, L. Picado-Santos, J. Neves, S. Capitão, A review of nanomaterials' effect on mechanical performance and aging of asphalt mixtures, Appl. Sci. 9 (18) (2019) 3657.
[70] M. Hafeez, N. Ahmad, M. Kamal, J. Rafi, M. Haq, Jamal, S. Zaidi, M. Nasir, Experimental investigation into the structural and functional performance of graphene nano-platelet (GNP)-doped asphalt, Appl. Sci. 9 (4) (2019) 686.
[71] S. Wu, O. Tahri, State-of-art carbon and graphene family nanomaterials for asphalt modification, Road. Mater. Pavement Des. 22 (4) (2019) 735–756.
[72] X. Li, Y. Wang, Y. Wu, H. Wang, M. Chen, H. Sun, L. Fan, Properties and modification mechanism of asphalt with graphene as modifier, Constr. Build. Mater. 272 (2021), 121919.
[73] F. Moreno-Navarro, M. Sol-Sánchez, F. Gámiz, M. Rubio-Gámez, Mechanical and thermal properties of graphene modified asphalt binders, Constr. Build. Mater. 180 (2018) 265–274.
[74] C. Fang, R. Yu, S. Liu, Y. Li, Nanomaterials applied in asphalt modification: a review, J. Mater. Sci. Technol. 29 (7) (2013) 589–594.
[75] J. Yang, S. Tighe, A review of advances of nanotechnology in asphalt mixtures, Procedia Soc. Behav. Sci. 96 (2013) 1269–1276.
[76] S. Goh, M. Akin, Z. You, X. Shi, Effect of deicing solutions on the tensile strength of micro- or nano-modified asphalt mixture, Constr. Build. Mater. 25 (1) (2011) 195–200.
[77] M. Khattak, A. Khattab, H. Rizvi, P. Zhang, The impact of carbon nano-fiber modification on asphalt binder rheology, Constr. Build. Mater. 30 (2012) 257–264.
[78] V. Hemanth Kumar, S. Suresha, Investigation of aging effect on asphalt binders using thin film and rolling thin film oven test, Adv. Civ. Eng. Mater. 8 (1) (2019), 20190119.
[79] J. Wang, Z. Chen, B. Chen, Adsorption of polycyclic aromatic hydrocarbons by graphene and graphene oxide nanosheets, Environ. Sci. Technol. 48 (9) (2014) 4817–4825.
[80] E. Pérez, N. Martín, Π–Π interactions in carbon nanostructures, Chem. Soc. Rev. 44 (18) (2015) 6425–6433.
[81] I. Fortelný, J. Kovář, Theory of coalescence in immiscible polymer blends, Polym. Compos. 9 (2) (1988) 119–124.
[82] D. Lesueur, J. Gerard, P. Claudy, J. Letoffe, Relationships between the structure and the mechanical properties of paving grade asphalt cements, J. Assoc. Asph. Paving Technol. 66 (1997) 486–519.
[83] M. Kane, M. Do, Tribological approach to study polishing of road surface under traffic, Tribol. Mater., Surf. Interfaces 1 (4) (2007) 203–210.
[84] J. Rahul, M. Jain, An investigation in to the impact of particulate matter on vegetation along the national highway: a review, Res. J. Environ. Sci. 8 (7) (2014) 356–372, 356-37.